

# CURRENT-ENHANCED SASE USING AN OPTICAL LASER AND ITS APPLICATION TO THE LCLS\*

A.A. Zholents, W.M. Fawley<sup>†</sup>, LBNL, Berkeley, CA 94720-8211, USA  
 P. Emma, Z. Huang, G. Stupakov, SLAC, Stanford, CA 94309, USA  
 S. Reiche, UCLA, Los Angeles, CA 90095-1547, USA

## Abstract

We propose a significant enhancement of the electron peak current entering a SASE undulator by inducing an energy modulation in an upstream wiggler magnet via resonant interaction with an optical laser, followed by microbunching of the energy-modulated electrons at the accelerator exit. This current enhancement allows a reduction of the FEL gain length. The x-ray output consists of a series of uniformly spaced spikes, each spike being temporally coherent. The duration of this series is controlled by the laser pulse and in principle can be narrowed down to just a single,  $\sim 200$ -attosecond spike. Given potentially absolute temporal synchronization of the x-ray spikes to the energy-modulating laser pulse, this scheme naturally makes pump-probe experiments available to SASE FEL's. We also study various detrimental effects related to the high electron peak current.

## INTRODUCTION

SASE-based x-ray FEL projects continue to gather momentum at SLAC[1] and DESY[2]. Recently, Ref. [3] has proposed a technique (which we call current-Enhanced SASE or ESASE for short) to shorten the exponential gain length and provide temporal synchronization of the x-ray pulse to a master laser. Figure 1 shows a schematic of this technique as applied to the LCLS. An external, short pulse ( $\sim 30$ -100 fs) from a high power ( $\sim 1$ -10 GW) laser at wavelength  $\lambda_L \sim 2.2 \mu\text{m}$  (e.g. TOPAS laser [4]) overlaps a short e-beam section at moderate energy ( $\sim 4.5$  GeV) in a short, appropriately-tuned wiggler (e.g.  $\lambda_u \approx 30$  cm,  $B_u \approx 1.7$  T). This induces a periodic energy modulation with relative amplitude  $B \equiv \Delta\gamma/\sigma_{\gamma 0} \sim 5$ -10, where  $\sigma_{\gamma 0}$  is the uncorrelated energy spread, but with minimal microbunching. Following final acceleration the electron beam passes through a dog-leg bend whose chromatic dispersion produces a periodic enhancement of the peak current to  $\approx 20$  kA. Finally, the electrons enter a long undulator and emit x-rays via the standard SASE process but with first saturation occurring by  $z \approx 45$ -60 m. The radiation output from the current-enhanced portions will be a train of spikes at uniform spacing  $\lambda_L$  whose total duration is directly related to that of the upstream, energy-modulating laser. This emission will dominate SASE emis-

sion from the remainder of the e-beam if the exponential gain lengths in the current spikes have been reduced by  $\approx 25\%$  or greater.

The ESASE technique shares with other recent proposals [5, 6, 7] the common feature of employing an optical laser to induce energy modulation to produce short duration ( $\tau_P \leq 500$  as) output pulses from an FEL together with absolute synchronization of the x-ray probe pulse to the laser pump pulse, thus permitting pump-probe experiments. In principle, it is also related to harmonic cascade configurations [8]. However, via the use of a dispersion section to strongly enhance the current, ESASE has the additional advantage of significantly reduced gain lengths. This may allow possible relaxation of the required electron beam emittance for saturation in the "standard" LCLS undulator or (for the same base emittance) saturation at x-ray wavelengths shorter than 0.15 nm.

We now present initial "start-to-end" numerical simulation results, investigate some potential detrimental effects due to the high peak currents, and then conclude with some remarks concerning possible experimental applications.

## ACCELERATOR SIMULATIONS

We initiated "start-to-end" ESASE simulations with  $2 \times 10^5$  macro-particles in the *Parmela*[9] code for the RF photo-cathode gun and low-energy injector systems, up to an energy of 135 MeV. After this point, the macroparticle number is increased  $10\times$ , retaining all second moments and coordinate correlations, and then transported with the *Elegant*[10] code through the main linac, up to the entrance of the FEL undulator. These simulations included 2nd-order optics, accelerating structure wakefields, a model for the laser/wiggler energy modulator (EM) at 4.54 GeV, and a line-charge (1D) model of coherent synchrotron radiation (CSR) in and after the bends.

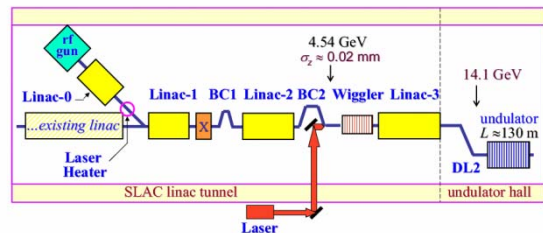


Figure 1: A schematic of ESASE as applied to the LCLS.

\* Work supported in part by the Office of Science, U.S. Dept. of Energy under Contracts DE-AC03-76SF0098 and DE-AC03-76SF00515.

<sup>†</sup> WMFawley@lbl.gov

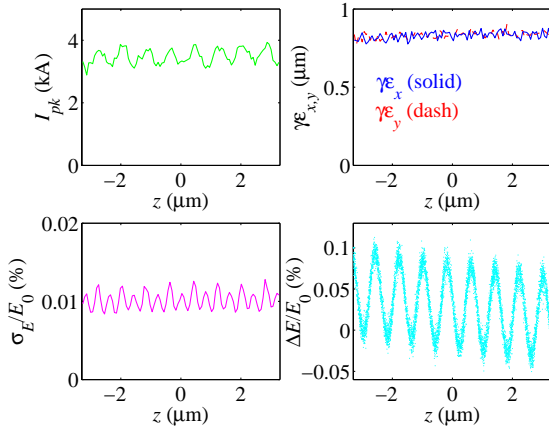


Figure 2: ELEGANT tracking results for a short section of 0.8- $\mu\text{m}$  energy-modulated  $e^-$  bunch at 14 GeV, with instantaneous current, transverse emittances, rms relative energy spread, and relative energy centroid modulation plotted versus bunch coordinate  $z$ .

The EM consists of a resonant laser-electron interaction in an 2.5-m long planar wiggler located immediately after the second bunch compressor chicane where the FWHM bunch length is 65  $\mu\text{m}$ . The EM can easily be installed in place of one existing 3-m long accelerating structure. Table 1 gives the EM and the final buncher parameters.

Figure 2 displays the resulting current profile, transverse slice emittance, rms energy spread, and centroid energy modulation induced by an 0.8- $\mu\text{m}$  wavelength EM for a short core-section of the beam at 14.1 GeV. The current profile shows weak density modulation due to the wiggler's small momentum compaction (opposite in sign to the final buncher). Similar weak modulation of  $\sigma_E$  is also apparent.

Following final acceleration, the beam passes through a 'dog-leg' transport line (DL2) which is used to produce a 1.25-m jog in the beamline to the south, in order to allow energy measurement and collimation. The DL2 beamline nominally has a very small momentum compaction of  $R_{56} \approx 0.1$  mm, but it can be easily increased, or even reversed in sign, by small adjustments in the gradients of three nearby quadrupole magnets. For the energy modulation shown in Fig. 2,  $R_{56} = 0.30$  mm is optimum. Fig. 3 shows the beam characteristics immediately following this bend system, including CSR effects.

CSR calculations require both a large number of macro-

Table 1: Energy modulator (EM) at 4.54 GeV for  $B=5$  and two laser wavelengths ( $\lambda_L = 0.8 \mu\text{m}$  and  $2.2 \mu\text{m}$ ).

Parameter	sym	0.8 $\mu\text{m}$	2.2 $\mu\text{m}$	unit
$N$ wiggler periods	$N_w$	8	8	—
period of wiggler	$\lambda_w$	25	30	cm
peak laser power	$P_{pk}$	9.7	10.7	GW
laser rms waist	$\sigma_r$	0.25	0.25	mm
modulation amp.	$\Delta\gamma$	$\pm 14$	$\pm 14$	—
buncher $R_{56}$	$R_{56}$	0.30	0.78	mm

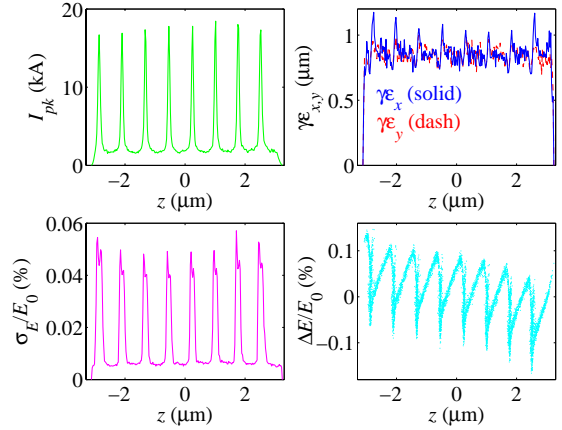


Figure 3: Same plots as in Fig. 2, but at a  $z$ -position immediately following the DL2 beamline. Strong current modulation and CSR effects are now apparent.

particles and narrow bin width ( $\sim 6$  nm) due to the short ESASE bunching length ( $\approx 30$  nm rms). This spike length still greatly exceeds the CSR point-charge wake limit of  $R/\gamma^3 \approx 0.01$  nm at 14 GeV for bends with radius  $R \approx 300$  m [11]. It is worth noting that the CSR in the DL2 dipoles will be partially suppressed by a combination of a non-zero  $R_{51}$  component and a relatively large transverse beam size. The projected spike length in the bends along the axis of propagation will broaden to  $\sigma_x|\theta| \approx 400$  nm, where  $\sigma_x \approx 45 \mu\text{m}$  is the rms horizontal beam size at the bend entrance and  $\theta \approx 0.5^\circ$  is the bend angle. This longer effective length, the low charge in each spike, and the weak bend angles all minimize CSR effects, although a 20% horizontal emittance growth and some phase space distortion is still evident in Fig. 3. Nonetheless, a fully 3D CSR calculation is needed to verify these 1D results.

## FEL SIMULATION RESULTS

The 6D macroparticle distributions resulting from the ELEGANT tracking studies were directly imported as input to the FEL simulation codes *GINGER*[12] and *GENESIS*[13]. We performed a number of fully time-dependent ( $\Delta t_{\text{slice}} \sim 10$  as) SASE runs at two different energy modulation wavelengths (0.8 and 2.2  $\mu\text{m}$ ) and two undulator focusing lattices ( $\langle\beta\rangle = 26$  and 12 m) with the standard LCLS  $\lambda_u = 30$  mm undulator period. For these calculations wakefield effects were neglected. Table 2 sum-

Table 2: Simulation results from GINGER and GENESIS.

Param.	$\langle\beta\rangle = 26$ m		$\langle\beta\rangle = 12$ m		unit
$\lambda_L$	STD	0.8	2.2	0.8	2.2
$L_{\text{sat}}$	70	58	57	44	45
$\langle P \rangle$	13	2.0	3.0	2.9	7.6
$P_{\text{spike}}$	240	17	65	40	160
$\omega/\Delta\omega$	1500	550	660	660	790

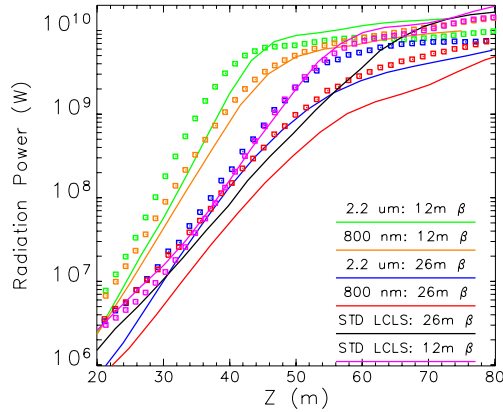


Figure 4:  $\langle P \rangle$  plotted versus  $z$  for ESASE and standard LCLS configurations. The solid lines and boxes represent *GINGER* and *GENESIS* results, respectively.

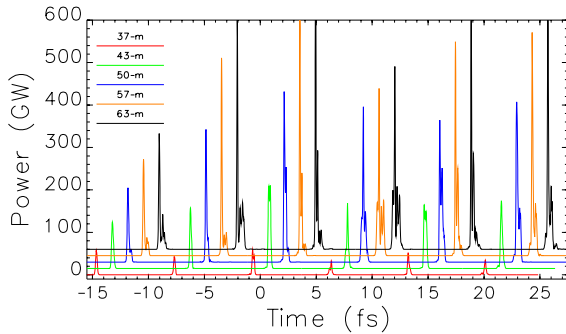


Figure 5:  $P(t)$  snapshots at 5 different  $z$ -locations for a  $2.2\text{ }\mu\text{m}$ -energy-modulated ESASE pulse with  $\langle \beta \rangle = 12\text{ m}$ , plotted with staggered offsets of  $1.5\text{ fs}$  in time and  $15\text{ GW}$  in power. For legibility, the  $z=37\text{ m}$  data has been multiplied by a factor of 2.0.

marizes various output parameters from the simulations. For simplicity, we have defined the saturation point as that where the normalized inverse spectral bandwidth  $\omega/\Delta\omega$  reaches a maximum and  $P_{\text{spike}}$  as the average peak power of the spikes measured at  $z = L_{\text{sat}}$ . The ESASE results show significantly reduced saturation lengths, albeit with somewhat smaller average powers and inverse bandwidths than the “standard” LCLS configuration. In particular, if it were possible to achieve an  $\langle \beta \rangle = 12\text{ m}$  or less,  $L_{\text{sat}}$  is reduced to less than  $50\text{ m}$ . We believe the enhanced gain from such an ESASE configuration would allow the LCLS to operate at a somewhat larger normalized emittance than the nominal  $1.2\text{ mm-mrad}$  or at somewhat shorter wavelengths than the nominal  $0.15\text{ nm}$ . The time-averaged powers for both the ESASE cases and standard LCLS parameter cases (“STD”) are shown in Fig. 4. Because *GENESIS* unlike *GINGER* includes non-axisymmetric modes, in the early regions of exponential gain it will tend to show a significantly higher power.

One important feature of the ESASE runs is that the instantaneous power is essentially composed of simple,

uniformly-spaced spikes with effective widths  $\leq 0.5\text{ fs}$  up to and about one-to-two gain lengths beyond  $L_{\text{sat}}$ . Between the individual spikes, the instantaneous SASE power is smaller by three orders of magnitude or greater. As predicted by Ref. [14] for SASE in the short pulse limit, the individual spikes support a single coherent longitudinal mode and their bandwidth is approximately transform-limited for  $z \leq L_{\text{sat}}$  (presuming one has matched  $\lambda_L/B$  to approximately one coherence length). Fig. 5 shows  $P(t)$  snapshots at various  $z$ -locations for a  $2.2\text{-}\mu\text{m}$  laser-modulated pulse with  $\langle \beta \rangle = 12\text{ m}$ . At  $z=57\text{ m}$ , approximately three gain lengths beyond saturation, some spikes begin to display multi-peak structure and pulse widths approaching  $1\text{-fs}$  or greater due to slippage effects.

## COLLECTIVE EFFECTS

The high peak current in the ESASE spikes raises concerns that impedance effects may induce sufficient energy spread to seriously degrade FEL performance. We now estimate the effects from three different sources.

### Wakefield Effects

The longitudinal resistive wall wake of high-current spikes will be partially suppressed by the large catch up distance  $z_c$  associated with the short spike length. Indeed, for  $\sigma_{\text{spike}}=30\text{ nm}$  and undulator pipe radius  $a=2.5\text{ mm}$ , we find  $z_c = a^2/2\sigma_{\text{spike}} \approx 100\text{ m}$ , which exceeds the expected FEL saturation length. Due to the finite beam  $\gamma$ , the extension of the image charge induced on the wall by a single spike,  $a/\gamma \approx 100\text{ nm}$ , is larger than  $\sigma_{\text{spike}}$ . This somewhat reduces  $z_c$ . However, even without this reduction, the wake induced by a single spike inside itself is expected to be small due to the small charge of the spike ( $\sim O(10)\text{ pC}$ ). If we take for the wake the value  $w = Z_0 c/\pi a^2$  (the limit of the steady state wake for very short bunches; see, e.g. Ref. [15]) where  $Z_0=377\Omega$  is the vacuum impedance, we estimate the induced energy spread in the spike due to this wake will be  $\delta E/E \approx 4 \times 10^{-4}$  at  $z=100\text{ m}$ . This is smaller than the intrinsic energy spread  $\sigma_E$  of the ESASE spike and should only slightly affect FEL performance.

The total charge in the spikes is a relatively small fraction of the total charge of the bunch. This means that the average wake of multiple spikes will be dominated by the averaged smooth current distribution in the bunch. This wake is not supposed to generate excessive energy spread in the beam.

### Coherent Undulator Radiation

Coherent undulator radiation (CUR) at wavelengths comparable to the spike length ( $\sim 30\text{ nm}$ ) but much longer than the resonant FEL wavelength  $\lambda_r = 2\pi/k_r$  ( $=0.15\text{ nm}$ ) can be an important impedance source. The CUR impedance per unit length at wavenumber  $k$  for a long

pencil beam is [16, 17]

$$Z_{CUR}^{1D}(k) = \frac{Z_0}{4\pi} \frac{K^2}{\gamma^2} \frac{k}{8} \left( 2\pi + 4i \ln \frac{k_r}{k} \right), \quad (1)$$

where  $K$  is the undulator parameter. However, long-wavelength undulator radiation is emitted primarily off-axis at an angle  $\theta \approx \sqrt{2\lambda/\lambda_u} \sim 1$  mrad. Consequently, the effective radiation impedance taking into account the transverse size of the bunch is modified to

$$Z_{CUR}^{3D} \approx Z_{CUR}^{1D} e^{-k^2 \theta^2 \sigma_x^2} = Z_{CUR}^{1D} e^{-2kk_u \sigma_x^2}. \quad (2)$$

with  $k_u \equiv 2\pi/\lambda_u$ . For an infinite train of ESASE bunches spaced by laser wavelength  $\lambda_L$ , the modulated electron current is (see e.g., Ref. [8])

$$I(z) = I_0 \left( 1 + 2 \sum_{n=1}^{\infty} J_n(nk_L R_{56} B \sigma_\delta) \times \exp \left[ -n^2 k_L^2 R_{56}^2 \sigma_\delta^2 / 2 \right] \cos(nk_L z) \right), \quad (3)$$

where  $I_0=3.4$  kA is the unmodulated beam current,  $J_n$  is the Bessel function of order  $n$ ,  $k_L = 2\pi/\lambda_L$ ,  $z$  is the longitudinal position along the bunch, and  $\sigma_\delta \equiv \sigma_{\gamma 0}/\gamma$  is the normalized rms energy spread. At the optimal compression  $k_L R_{56} B \sigma_\delta \approx 1$ , the energy loss per unit length is

$$\frac{d(\Delta\gamma)}{ds} \approx -\frac{2I_0}{I_A} \frac{K^2}{\gamma^2} \sum_{n=1}^{\infty} J_n(n) \exp \left[ -\frac{n^2}{2B^2} - 2k_n k_u \sigma_x^2 \right] \times \left[ \frac{\pi k_n}{4} \cos(2\pi n \bar{z}) - \frac{k_n}{2} \ln \left( \frac{k_r}{k_n} \right) \sin(2\pi n \bar{z}) \right], \quad (4)$$

where  $I_A \approx 17$  kA is the Alfvén current,  $k_n \equiv nk_L$  and  $\bar{z} \equiv z/\lambda_L$ . For  $B=5$ ,  $\lambda_L=0.8\mu\text{m}$ , and  $\gamma = 2.8 \times 10^4$  and  $\sigma_x=33\mu\text{m}$  in the undulator, Eq. (4) yields maximum  $d(\Delta\gamma)/ds \approx 0.003\text{ m}^{-1}$ , more than two orders of magnitude smaller than that obtained using the 1-D CUR impedance (i.e., Eq. (1)).

### Longitudinal Space Charge Effects

Another high-frequency impedance is the longitudinal space charge (LSC). Since  $k_n \sigma_x/\gamma \ll 1$  (pencil beam in the rest frame) and  $k_n a/\gamma \gg 1$  for all  $n$  except  $n = 1$  at  $\lambda_L=0.8\mu\text{m}$ , we use the free-space LSC impedance per unit length (see, e.g., Ref. [18]):

$$Z_{LSC}(k) \approx i \frac{Z_0}{4\pi} \frac{k}{\gamma^2} \left( 1 + 2 \ln \frac{\gamma}{k(\sigma_x + \sigma_y)} \right). \quad (5)$$

For  $B=5$ ,  $\lambda_L=0.8\mu\text{m}$ , and  $\sigma_x=33\mu\text{m}$ , we find that the maximum  $d(\Delta\gamma)/ds \sim 0.1\text{ m}^{-1}$ . For  $\lambda_L=2.2\mu\text{m}$ ,  $d(\Delta\gamma)/ds \sim 0.05\text{ m}^{-1}$ . For the  $\approx 200$ -m long diagnostic section between DL2 and the undulator, the space-charge-induced growth in  $\Delta\gamma$  to  $O(20)$  is large enough for concern. If necessary, the current bunching could be delayed by making the DL2 dogleg isochronous together with installation of a weak chicane just before the undulator. Over the 100-m length of the undulator, the space-charge-induced energy spread increase is less than that of the spikes's initial value  $\sigma_E$ .

## CONCLUDING REMARKS

The ESASE technique allows obtaining electron beam micro-bunches with a peak current unthinkable from a standard electron bunch compressor. Our preliminary investigations suggest that the high peak currents induce only limited beam quality degradation due to collective effects such as CSR, wakefields, and space charge; nonetheless more detailed studies are needed for greater certainty. Although the exponential ESASE gain length is only somewhat shortened relative to an unmodulated beam for the standard LCLS undulator with  $\beta=26$  m, there is a much shorter gain length and more rapid saturation in  $z$  for  $\beta=12$  m. For this latter case, detailed “start-to-end” simulations show that the output SASE x-ray pulse will be dominated by periodic spikes of a few hundred attosecond or less duration. Consequently, the duration of the overall output envelope can be controlled by adjusting the modulating laser pulse. One can also obtain absolute synchronization between these two pulses which can be used in the pump-probe experiments for ultra-fast dynamics studies at the femtosecond time scale and beyond. We plan further studies to explore more fully the potential of ESASE techniques at the LCLS.

## REFERENCES

- [1] LCLS Conceptual Design Report, SLAC-R-593 (2002).
- [2] TESLA Technical Design Report, DESY TESLA-FEL 2001-05 (2001).
- [3] Zholents, A.A., submitted to *Phys. Rev. Lett.* (2004)
- [4] <http://www.lightcon.com/lc/scientific/topas.htm>
- [5] Zholents, A.A. and Fawley, W.M., *Phys. Rev. Lett.* **92**, 224801 (2004).
- [6] Saldin, E.L., Schneidmiller, E.A., and Yurkov, M.V., *Opt. Comm.*, **237**, 153 (2004)
- [7] Saldin, E.L., Schneidmiller, E.A., and Yurkov, M.V., *Opt. Comm.*, in press, (2004)
- [8] L.H. Yu, *Phys. Rev. A*, **44**, 5178 (1991).
- [9] J. Billen, LANL Report LA-UR-96-1835 (1996).
- [10] M. Borland, ANL report APS LS-287 (2000).
- [11] E.L. Saldin, E.A. Schneidmiller, and M.V. Yurkov, *Nucl. Inst. Meth. A*, **398**, 373 (1997).
- [12] W.M. Fawley, LBNL-49625 (2002).
- [13] S. Reiche, *Nucl. Inst. Meth. A*, **429**, 243 (1999).
- [14] R. Bonifacio *et al.*, *Phys. Rev. Lett.* **73**, 70 (1994).
- [15] K.L.F. Bane and M. Sands, SLAC-PUB-95-7074 (1995).
- [16] E.L. Saldin, E.A. Schneidmiller and M.V. Yurkov, *Nucl. Instrum. Meth. A*, **417**, 158 (1998).
- [17] J. Wu, T. Raubenheimer, G. Stupakov, *Phys. Rev. ST Accel. Beams*, **6**, 040701 (2003).
- [18] A. Chao, *Physics of Collective Beam Instabilities in High Energy Accelerators* (Wiley, New York, 1993).